ELSEVIER

Chemical Geology 126 (1995) 77–99

CHEMICAL GEOLOGY
INCLUDING
ISOTOPE GEOSCIENCE

# Alteration of basalt hyaloclastite at the off-axis Sea Cliff hydrothermal field, Gorda Ridge

R.A. Zierenberg [a,*], P. Schiffman [b], I.R. Jonasson [c], R. Tosdal [a], W. Pickthorn [a], J. McClain [b]

[a] *U.S. Geological Survey, 345 Middlefield Rd. MS 901, Menlo Park, CA 94025, USA*
[b] *Department of Geology, University of California, Davis, CA 95616, USA*
[c] *Geological Survey of Canada, 601 Booth St., Ottawa, Ont. K1A 0E8, Canada*

Received 1 January 1995; accepted 31 July 1995

**Abstract**

The Sea Cliff hydrothermal field on the northern segment of the Gorda Ridge is situated along a rift-bounding normal fault about 2.6 km east of the neovolcanic zone and approximately 300 m above the spreading axis. The structural setting of this hydrothermal field differs from that of most other active seafloor hydrothermal sites investigated to date, which are typically situated in the neovolcanic zone. Mineralization occurs in basaltic talus covering a large normal-fault scarp. Hydrothermal crusts cover much of the seafloor in the area of the active hydrothermal field. These crusts form by extensive alteration of basaltic hyaloclastite in a zone of mixing between ascending hydrothermal fluid and entrained seawater. The initial stage of alteration is magnesian metasomatism of both crystalline basalt and basaltic glass, converting the rock to Mg-rich smectite and smectite/chlorite. Further alteration removes nearly all cations and ultimately leads to silicification. Preservation of basaltic texture in the silicified rocks provides evidence that even such sparingly soluble elements as Al and Ti have been removed. Oxygen-isotopic ratios of the altered rocks constrain initial alteration to temperatures near 220°C, close to the maximum measured vent temperatures of 247°C. Silicification proceeded to much lower temperatures, and most amorphous silica deposition occurred at temperatures below 100°C. Sulfur-, strontium-, and lead-isotopic data all indicate a predominantly basaltic source, with important contributions from seawater but no significant contribution from sedimentary sources. Comparison with ophiolite-hosted massive sulfide deposits shows that the structural setting, alteration sequence, and depositional environment are all similar and suggests that mineralization and replacement of basaltic breccia in the Sea Cliff hydrothermal field likely occur in the subsurface beneath a capping layer of silicified hyaloclastite.

## 1. Introduction

### *1.1. Geologic setting*

The Gorda Ridge spreading center is bounded on the north by the Blanco Fracture Zone and on the south by the Mendocino Fracture Zone (Fig. 1). The northern third of the Gorda Ridge is a continuous second-order ridge segment (Macdonald et al., 1991) bounded on the south by a right-lateral discontinuity at 42°25'N (Clague and Holmes, 1987). Although the northern segment of the Gorda Ridge has a full spreading rate of 55 mm/yr (Riddihough, 1980), similar to the Cleft segment of the Juan de Fuca Ridge to the north, the Gorda Ridge has the morphology of a slowly spreading ridge. The axial valley on its northern segment deepens

* Corresponding author.

0009-2541/95/$09.50 © 1995 Elsevier Science B.V. All rights reserved
*SSDI* 0009-2541(95)00111-5

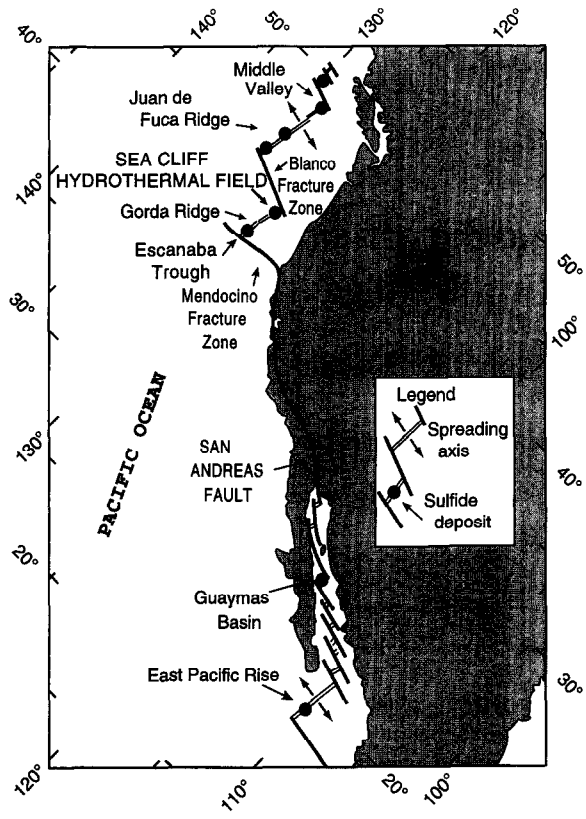


Fig. 1. Northeastern Pacific Ocean, showing major tectonic boundaries and the location of Sea Cliff hydrothermal field.

systematically from 3050 m at the shoal point near lat 42°44′N, to more than 3750 m at the ridge-transform intersection to the north. The axial valley is narrowest (~3 km wide) near the midsegment axial high and widens to approximately 10 km to the north and south (Clague and Rona, 1990), giving the ridge segment an hourglass shape typical of Mid-Atlantic Ridge segments. The axial valley is flanked by steep, normal fault-bounded ridges that rise to about 2400 m, typically in a series of four 1-km-wide steplike terraces that define the outward-tilted fault blocks (Atwater and Mudie, 1973).

### 1.2. Previous work

Water-column surveys of the Gorda Ridge revealed temperature, light-attenuation, $^3$He, and dissolved-manganese anomalies indicative of hydrothermal discharge near 42°44.7′N 126°43.7′W, at a site originally designated GR-14 (Collier et al., 1986; Baker et al., 1987; Collier and Baker, 1990). Anhydrite was identified among particulate matter filtered from water samples, indicating the presence of moderate- to high-temperature hydrothermal discharge (Baker et al., 1987). The distribution of water-column anomalies suggested that hydrothermal discharge was occurring approximately 2.6 km east of the spreading axis on a fault-block terrace that is about 300 m above the axial-valley floor (Fig. 2). The source of this discharge was inferred to be near the south end of a 0.5-km-wide, 1-km-long ridge that rises more than 100 m above the western scarp of the terrace (Baker et al., 1987). Extrapolation of the present spreading rate indicates that the hydrothermal site is on 100,000-yr-old crust.

Geologic and geophysical mapping also pointed to the off-axis ridge at site GR-14 as the likely site of hydrothermal discharge. Side-scan-sonar mapping

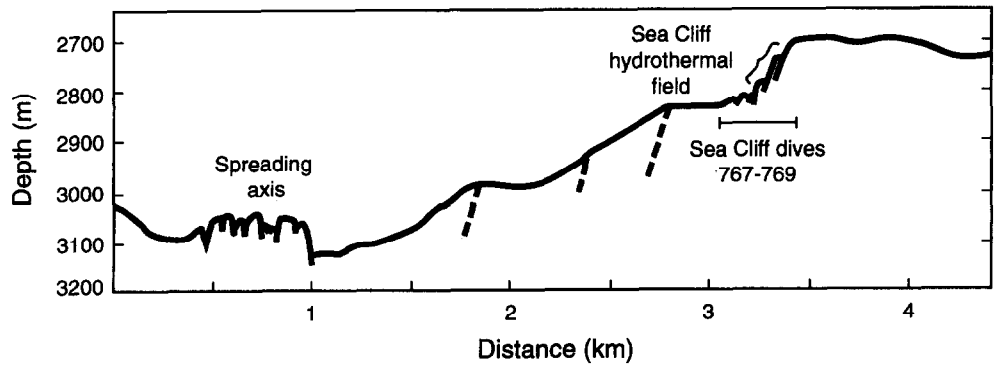


Fig. 2. Cross-section of Gorda Ridge spreading center, showing location of Sea Cliff hydrothermal field above axial valley along ridge-bounding normal fault (after Rona et al., 1990).

indicated that ridge-axis-parallel faults and fissures trending 022° are intersected by a set of off-axis faults and fissures trending 350° in the area of the water-column anomalies, leading to speculation that the location of hydrothermal venting may be structurally controlled (Rona and Clague, 1989; Clague and Rona, 1990). Camera tows near site GR-14 failed to locate active hydrothermal venting but did image areas of hydrothermal alteration and sedimentation both on axis and at the south end of the off-axis ridge that was the suspected site of hydrothermal discharge (Rona and Clague, 1989; Clague and Rona, 1990). Subsequent flow are characterized by clumps of tubeworms and other vent-specific biota growing on basaltic talus. The talus is stained with hydrothermal minerals (Rona et al., 1990), and discharged fluids produce shimmering water. Collinear clumps of tubeworms were observed along at least one of the steeper, faulted walls in the hydrothermal field, suggesting that fluid flow is controlled by fracture permeability. Such fracture permeability may underlie the entire field (e.g., Rona and Clague, 1989), but on gentler slopes it is obscured and fluid flow is defocused by the overlying talus and sediment.

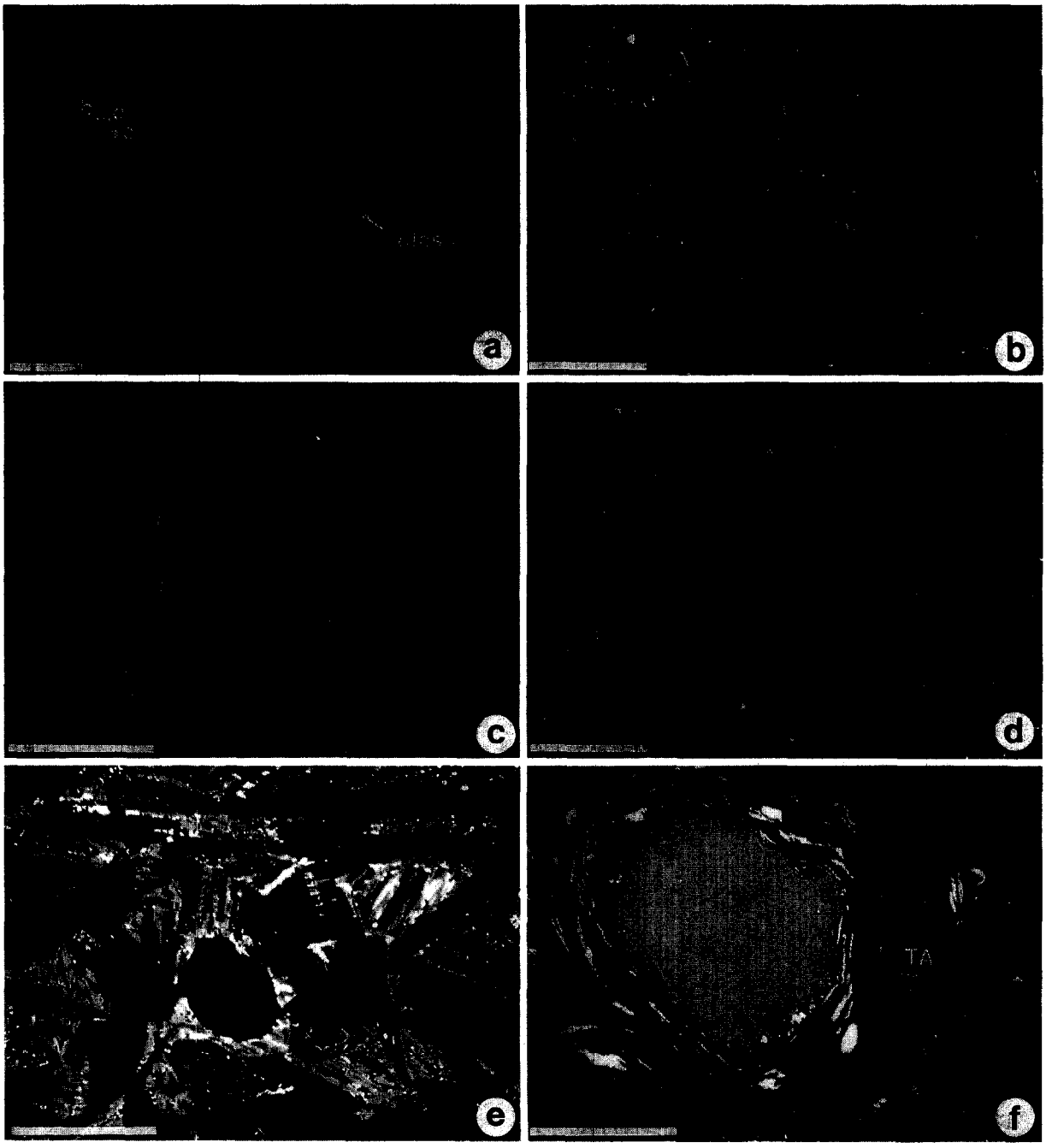


Fig. 4. Relic basaltic textures in hydrothermal crusts. (a) Cut slab of sample 769-1, showing large, altered, hyalocrystalline basaltic clast on left and smaller, fresh, glassy basaltic clast on right (labeled *glass*). Letters mark locations of (b), (c) and (d). Scale bar is 5 mm. (b) Core region of large basaltic clast in (a), containing fresh plagioclase and clinopyroxene, although intersertal groundmass is replaced by chlorite/smectite. BSE image; scale bar is 200 $\mu$m. (c) Sharp boundary between zones of relic and recrystallized textures on margin of large basaltic clast in (a). In relic zone on right, clinopyroxene (light) is fresh, and plagioclase and groundmass (gray) are replaced by chlorite/smectite; in recrystallized zone on left, all relic phases are recrystallized to mixture of chlorite/smectite and silica, with marked increase in porosity. BSE

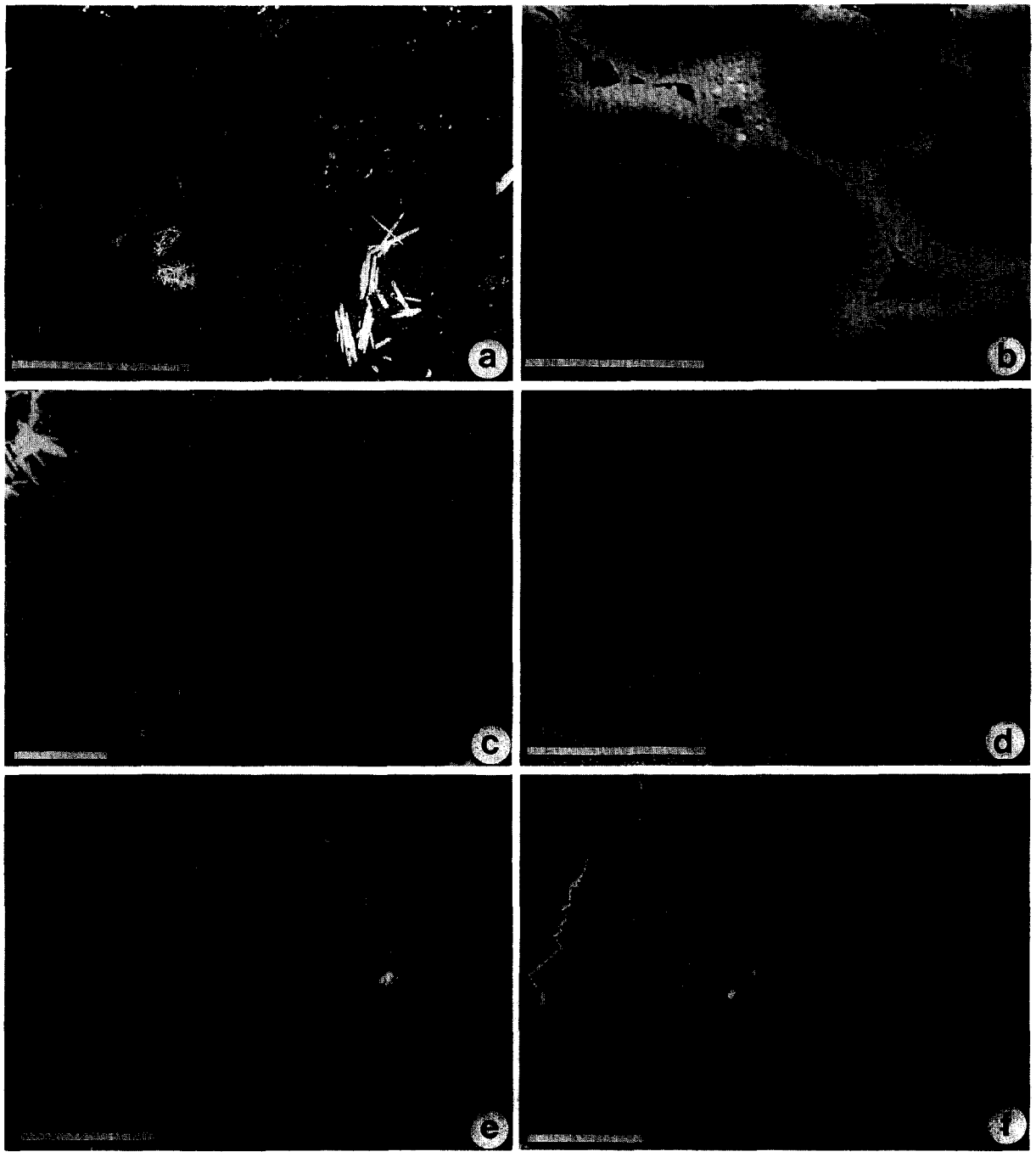


Fig. 5. BSE images of Mg- and Si-metasomatized, glassy basaltic clasts from Sea Cliff hydrothermal field and Turner-Albright ophiolite-hosted massive sulfide deposit. (a) Siliceous spherulitic clasts (dark with light rims) in matrix of amorphous silica, barite (bright, acicular crystals), and sulfides (disseminated, smaller, bright clots) (sample 769-1). Scale bar is 0.5 mm. (b) Closeup of spherulitic, siliceous clasts showing textural banding and relic, smectitic(?), fibrous textures (sample 769-1). Scale bar is 100 $\mu$m. (c) Angular glassy clast in sample 767-3. Darker core is composed of stevensite; gray layer about stevensitic core is composed of high-Al amorphous silica, which appears to have replaced original stevensite; lighter gray rim to clast is composed of low-Al amorphous-silica cement. Scale bar is 200 $\mu$m. (d) Al-K$\alpha$ X-ray dot map of

alteration zones, demonstrating that the alteration sequence is developed on a single fragment. Because the volcanic fragments typically are very highly altered and commonly semiopaque, the primary texture of the original fragments is best observed by BSE imaging (Fig. 4b–4f). For example, plagioclase microlites in the core of an approximately 5-mm-thick clast are unaltered (Fig. 4b), although adjacent intersertal groundmass is replaced by chlorite/smectite. Progressing a few millimeters toward the rim of the clast, plagioclase phenocrysts have also been replaced by chlorite/smectite, but the original intersertal texture is retained (Fig. 4d). Within the outer millimeter of the clast, however, a sharp reaction front subdivides this inner zone from an outer zone characterized by marked dissolution of the basalt and reprecipitation of saponite and silica (Fig. 4c). Variolitic zones and vesicles in quenched-textured basalt are typically the sites of initial saponitization and silicification (Fig. 4e).

The crust samples collected from the Sea Cliff hydrothermal field also contain a few other types of clasts, the least common of which are unaltered basaltic-glass fragments that are found in close proximity to highly altered glass fragments (Fig. 4a). Rare fragments with an apparent sedimentary origin were also observed, including some containing poorly preserved foraminifers. The rare massive sulfide fragments are predominantly pyrite and less abundant sphalerite and chalcopyrite. Rarely, the chalcopyrite shows minor alteration to covellite.

The hyalocrystalline basaltic clasts described above were likely derived from lava flows adjacent to the Sea Cliff hydrothermal field. A sample of an unaltered basaltic talus block (sample 769-2) collected near the hydrothermal field has an intersertal texture, with a groundmass of plagioclase microlites, interstitial clinopyroxene, and minor amounts of glass. Phenocrysts of clinopyroxene are less abundant than plagioclase phenocrysts and glomerocrysts. Plagioclase crystals have well developed oscillatory zoning that is locally truncated and overgrown, indicating partial resorption. The only alteration (weathering) evident in the basalt is local patches of yellow smectite in the glassy interstices.

The matrix of the fragments is predominantly amorphous silica and less abundant chalcedony. The most common texture is colloform to botryoidal banding (Fig. 5c). Many fragments are coated by banded amorphous silica. Barite in the matrix generally forms radiating clusters of bladed tabular crystals (Fig. 5a). Banded amorphous silica commonly coats these barite crystals. Amorphous-silica overgrowths preserve the outline of splays of elongate tabular crystals that have subsequently been dissolved. The shape of the crystal outlines is typical of anhydrite crystals formed in an active seafloor hydrothermal system. Minor amounts of pyrite occur in the matrix, generally as fine-grained disseminated cubes but also as framboids.

Microbial mats preserved in cavities near the original upper surface of the hydrothermal crust (Fig. 3d) contain a distinctive assemblage of sulfide minerals. Prior to the preservation of the microbial mats by silica encapsulation, most of the microbial filaments were selectively replaced by sulfides (Zierenberg and Schiffman, 1990), including pearcite ($Ag_{14.7-x}Cu_{1.3-x}As_2S_{11}$), proustite ($Ag_3AsS_3$), chalcopyrite, and galena. Except for chalcopyrite, however, these phases are not observed in the fragments of massive sulfide contained in the crusts, suggesting that microbial processes may have selectively precipitated silver and arsenic (Zierenberg and Schiffman, 1990). Some of the amorphous silica lining the cavities that contain microbial mats contains fluid inclusion filled with a yellow liquid interpreted to be hydrocarbon derived from thermal pyrolysis of microbial organic matter during hydrothermal alteration (Zierenberg and Schiffman, 1990)

## 6. Microprobe data

### 6.1. Amorphous silica and basaltic glass

Amorphous silica analyzed from two colorless to brown, spherulitic clasts from the hydrothermal crust

Fig. 5 (*continued*)
area in (b). Scale bar is 100 μm. (e) Glassy basaltic clast from hyaloclastite breccia within Turner-Albright deposit. Clast is composed of Fe-rich chlorite; black matrix material is quartz. Scale bar is 500 μm. (f) Spherulitic texture within chlorite-replaced, glassy clast within a hyaloclastite breccia from Turner-Albright deposit. Scale bar is 100 μm.

Table 1
Average composition of fresh basaltic glass and amorphous silica from hydrothermal crusts in the Sea Cliff hydrothermal field, in wt% from electron-microprobe analyses

| Sample: | 769-1 basalt glass (20)"[a] | 769-1-1 amorphous silica (4)"[a] | 769-1-2 amorphous silica (6)"[a] |
|---|---|---|---|
| $SiO_2$ | 50.43 | 89.52 | 90.32 |
| $TiO_2$ | 1.35 | 0.03 | 0.01 |
| $Al_2O_3$ | 15.57 | 3.64 | 3.20 |
| MgO | 8.19 | 0.67 | 0.57 |
| CaO | 11.75 | 0.23 | 0.21 |
| MnO | 0.16 | 0.03 | 0.03 |
| FeO | 8.93 | 0.24 | 0.48 |
| $Na_2O$ | 2.65 | 0.14 | 0.25 |
| $K_2O$ | 0.08 | 0.15 | 0.40 |
| Total | 99.11 | 94.64 | 95.47 |
| Mg/(Mg+Fe) | 0.62 | 0.83 | 0.67 |
| $TiO_2/Al_2O_3$ | 0.09 | 0.01 | 0.00 |

769-1: fresh glassy basaltic clast.
769-1-1: clear to brown banded spherulitic clast.
769-1-2: pale-brown spherulitic clast.
[a]"Number of analyses.

(similar to those shown in Fig. 5b from sample 769-1) contains approximately 90 wt% $SiO_2$ (Table 1, columns 2 and 3). Aluminum is the second most abundant cation, with $Al_2O_3$ content averaging between 3–4 wt%. MgO contents average 0.5–1.0 wt%, whereas CaO, FeO, $K_2O$, and $Na_2O$ contents all average 0.1–0.5 wt%. $TiO_2$ and MnO contents are both below 0.1 wt%.

Aside from silicon, the amorphous silica is depleted in virtually all elements relative to fresh basaltic glass from a rare clast in sample 769-1 (Table 1, column 1), except for potassium, which is enriched. The fresh basaltic glass has a $TiO_2/Al_2O_3$ ratio of approximately 0.1, whereas this ratio in the amorphous silica is close to 0, reflecting the nearly quantitative removal of Ti with respect to Al during alteration of the glass.

### 6.2. *Layer silicates*

Three types of layer silicates are recognized on the basis of their composition: smectite, chlorite/smectite, and talc (Table 2). With one exception, smectites are nearly end-member saponites, which, when recalculated on a 22-oxygen-formula-unit basis, are characterized by low Al content and sums of tetrahedral + octahedral cations that total very close to the ideal trioctahedral value of 14.0 (Fig. 6A). The uniformly Mg-rich composition of these saponites, with Mg/(Mg+Fe) ratios averaging 0.81–0.98 (Fig. 6B), and their extremely low interlayer charge (Table 2, columns 1–6) classify them as stevensite, compositionally similar to the saponites from hydrothermal chimneys and associated mounds within the Middle Valley of the northern Juan De Fuca Ridge (Percival and Ames, 1993). The composition of stevensite in samples from the Sea Cliff hydrothermal field appears to vary systematically in Al, Ca, and K contents as a function of the mode of occurrence. For example, in a hyalocrystalline basaltic clast from sample 769-1 (Fig. 4e), the contents of all three elements increase from stevensite replacing olivine (Table 2, column 1), through that replacing glassy groundmass (Table 2, column 3), to that precipitating from solution in vesicles (Table 2, column 2).

The only non-Mg-rich smectite analyzed was from a nonhydrothermally altered fragment of a mostly fresh, hyalocrystalline basalt (sample 769-2). This Fe-rich smectite also has appreciable K and Na contents (Table 2, column 7), suggesting that it may be a mixture of dioctahedral smectite and celadonite, possibly formed by oxidative weathering.

Layer silicates identified as interlayered chlorite/smectite (Table 2, columns 8–11) were found in two

Table 2
Electron-microprobe analyses of layer-silicate minerals from the Sea Cliff hydrothermal field and calculation of unit formula based on 22 oxygens

| Sample: | 769-1-1 | 769-1-2 | 769-1-3 | 767-3-1 | 767-3-2 | 767-3-3 | 769-2-1 | 768-3 | 769-1B-1 | 769-1B-2a | 769-1B-2b | 769-1B-3 |
|---|---|---|---|---|---|---|---|---|---|---|---|---|
| Analyses: | 6 | 5 | 6 | 2 | 11 | 6 | 10 | 6 | 1 | 1 | 1 | 1 |
| $SiO_2$ | 56.18 | 53.85 | 56.28 | 50.61 | 53.28 | 58.12 | 48.97 | 42.59 | 41.54 | 38.83 | 37.79 | 61.44 |
| $TiO_2$ | 0.04 | 0.05 | 0.06 | 0.03 | 0.02 | 0.01 | 0.04 | 0.04 | 0.11 | 0.01 | 0.03 | 0.04 |
| $Al_2O_3$ | 0.15 | 2.13 | 1.00 | 3.00 | 2.32 | 1.06 | 1.49 | 10.09 | 19.90 | 13.80 | 20.86 | 0.22 |
| MgO | 24.02 | 24.04 | 24.26 | 26.83 | 25.88 | 27.99 | 3.80 | 26.11 | 20.97 | 29.20 | 26.11 | 28.83 |
| CaO | 0.09 | 0.33 | 0.18 | 0.05 | 0.11 | 0.15 | 0.10 | 0.77 | 0.21 | 0.12 | 0.09 | 0.05 |
| MnO | 0.05 | 0.02 | 0.04 | 0.28 | 0.04 | 0.07 | 0.05 | 0.06 | 0.08 | 0.03 | 0.04 | 0.04 |
| FeO | 9.02 | 10.00 | 10.24 | 2.99 | 1.44 | 1.00 | 32.58 | 3.59 | 3.11 | 4.87 | 3.57 | 1.86 |
| $Na_2O$ | 0.06 | 0.10 | 0.07 | 0.46 | 0.70 | 0.15 | 1.03 | 0.17 | 0.33 | 0.29 | 0.22 | 0.07 |
| $K_2O$ | 0.06 | 0.47 | 0.27 | 0.28 | 0.26 | 0.04 | 4.35 | 0.12 | 0.47 | 0.14 | 0.23 | 0.04 |
| Total | 89.67 | 90.99 | 92.40 | 84.53 | 84.05 | 88.59 | 92.41 | 83.54 | 86.72 | 87.29 | 88.94 | 93.59 |
| Si | 7.91 | 7.57 | 7.76 | 7.43 | 7.74 | 7.94 | 7.83 | 6.41 | 5.96 | 5.69 | 5.37 | 7.98 |
| Al | 0.02 | 0.35 | 0.17 | 0.52 | 0.39 | 0.17 | 0.28 | 1.79 | 3.37 | 2.38 | 3.49 | 0.03 |
| Mg | 5.04 | 5.04 | 4.98 | 5.87 | 5.61 | 5.70 | 0.90 | 5.86 | 4.49 | 6.37 | 5.52 | 5.77 |
| Fe | 1.06 | 1.18 | 1.19 | 0.37 | 0.17 | 0.12 | 4.36 | 0.47 | 0.38 | 0.60 | 0.42 | 0.20 |
| Mn | 0.00 | 0.00 | 0.00 | 0.03 | 0.00 | 0.00 | 0.00 | 0.00 | 0.00 | 0.00 | 0.01 | 0.00 |
| Ti | 0.00 | 0.00 | 0.00 | 0.00 | 0.00 | 0.00 | 0.00 | 0.00 | 0.02 | 0.00 | 0.00 | 0.00 |
| Ca | 0.02 | 0.05 | 0.02 | 0.00 | 0.02 | 0.02 | 0.02 | 0.13 | 0.03 | 0.02 | 0.02 | 0.00 |
| K | 0.02 | 0.09 | 0.05 | 0.06 | 0.05 | 0.00 | 0.89 | 0.02 | 0.09 | 0.02 | 0.04 | 0.00 |
| Na | 0.02 | 0.03 | 0.02 | 0.13 | 0.20 | 0.04 | 0.31 | 0.05 | 0.09 | 0.08 | 0.06 | 0.02 |
| Sum | 14.10 | 14.31 | 14.20 | 14.41 | 14.18 | 14.00 | 14.61 | 14.75 | 14.43 | 15.16 | 14.93 | 14.03 |
| Sum-IL | 14.05 | 14.14 | 14.10 | 14.21 | 13.92 | 13.93 | 13.40 | 14.55 | 14.22 | 15.05 | 15.01 | 13.99 |
| Mg/(Mg+Fe) | 0.83 | 0.81 | 0.81 | 0.94 | 0.97 | 0.98 | 0.17 | 0.93 | 0.92 | 0.91 | 0.93 | 0.97 |

769-1-1: smectite after olivine phenocryst in hyalocrystalline basaltic clast in crust
769-1-2: smectite spherule in hyalocrystalline basaltic clast in crust
769-1-3: smectite after groundmass of hyalocrystalline basaltic clast in crust
767-3-1: green, highly birefringent smectite alteration of glassy clast in crust
767-3-2: white, opaque smectite alteration of glassy clast in crust
767-3-3: green, low-birefringent smectite alteration of glassy clast in crust
769-2: yellow, highly birefringent smectite/celadonite(?) within groundmass of mostly fresh hyalocrystalline basalt
768-3: chlorite/smectite alteration of groundmass in otherwise-fresh basalt sample
769-1B-1: chlorite/smectite alteration of glassy groundmass within core of basaltic clast in crust
769-1B-2a: chlorite/smectite alteration of glassy groundmass along outer margin of basaltic clast in crust
769-1B-2b: chlorite/smectite alteration of plagioclase along outer margin of basaltic clast in crust
769-1B-3: talc replacement of olivine phenocryst within basaltic clast in crust

samples; a generally fresh basalt fragment (768-3) and a clast of hyalocrystalline basalt within a hydrothermal-crust sample (769-1). Compositionally, chlorite/smectite from both samples plots close to the ideal 'mixing' line between trioctahedral smectite and chlorite (Fig. 6A), indicating formation at temperatures above 100°C (Schiffman and Fridleifsson, 1991).

These chlorite/smectites are as uniformly Mg-rich (Fig. 6B) as the saponites from the hydrothermal crusts. However, the Al content of chlorite/smectite from sample 769-1 apparently depends on local bulk composition. For example, chlorite/smectite replacing a plagioclase microphenocryst (Fig. 4d) contains approximately 6 wt% more $Al_2O_3$ than chlorite/smectite (with a comparable Mg/(Mg+Fe) ratio) replacing adjacent glassy groundmass, although this second chlorite/smectite also has a lower Al content than chlorite/smectite replacing glassy groundmass within

the core of the same basaltic clast (cf. analyses in Table 2, columns 9–11).

Talc intergrown with saponite and replacing an olivine phenocryst (Fig. 4f) within a basaltic clast in a hydrothermal-crust sample (769-1) contains approximately 1.9 wt% FeO (Table 2, column 12).

### 6.3. Sulfides

Pyrite and chalcopyrite from detrital (chimney?) fragments in the hydrothermal crusts are nearly stoichiometric in composition. Pyrite contains 0.1–0.8 wt% As; otherwise, Zn, Mn, As (in chalcopyrite) and Cu (in pyrite) contents are all generally less than 0.1 wt%. Sphalerite from the anhydrite-bearing chimney fragment contains approximately 3 wt% Fe.

### 6.4. Sulfates

Barite in the hydrothermal crusts contains varying amounts of both Sr and Ca. SrO contents range from approximately 0.6 to 6.4 wt%, and CaO contents from 0.01 to 0.8 wt%. Anhydrite from a chimney fragment contains approximately 0.3 wt% SrO and 0.06 wt% BaO.

## 7. Bulk chemical analyses

Relative to unaltered basalt, the hydrothermal crusts are highly enriched in $SiO_2$, BaO, and $SO_3$; cations, including $Al_2O_3$ and $TiO_2$, have been strongly depleted (Table 3). Similar results were reported by Fisk and Howard (1989). Trace elements are highly enriched in the crusts, particularly Ag, As, Au, Co, Cu, Pb, Sr, and Zn (Table 3). The enrichment in chalcophilic elements is consistent with the presence of massive sulfide fragments in the crust, and the Sr enrichment can be accounted for by solid solution in barite. The precious-metal content of these samples is surprisingly high considering the small amount of contained sulfide minerals. Gold grades, in particular, exceed those of most samples of seafloor massive sulfide, even though the crusts contain less than 5% sulfide.

To assess the relative mobility of elements during hydrothermal alteration of basalt hyaloclastite, we compared the chemical composition of the crusts, a dark clast with relic basaltic texture, and matrix material from sample 769, using the isocon method (Grant, 1986). Compositions were plotted relative to a sample of unaltered basalt (769-2) collected from the Sea Cliff hydrothermal field, assuming that it is representative of the protolith of the basaltic fragments in the altered hyaloclastite crust (Fig. 7). Elements that show no change in concentration will plot on the one-to-one line shown in Fig. 7, assuming that the bulk density is con-

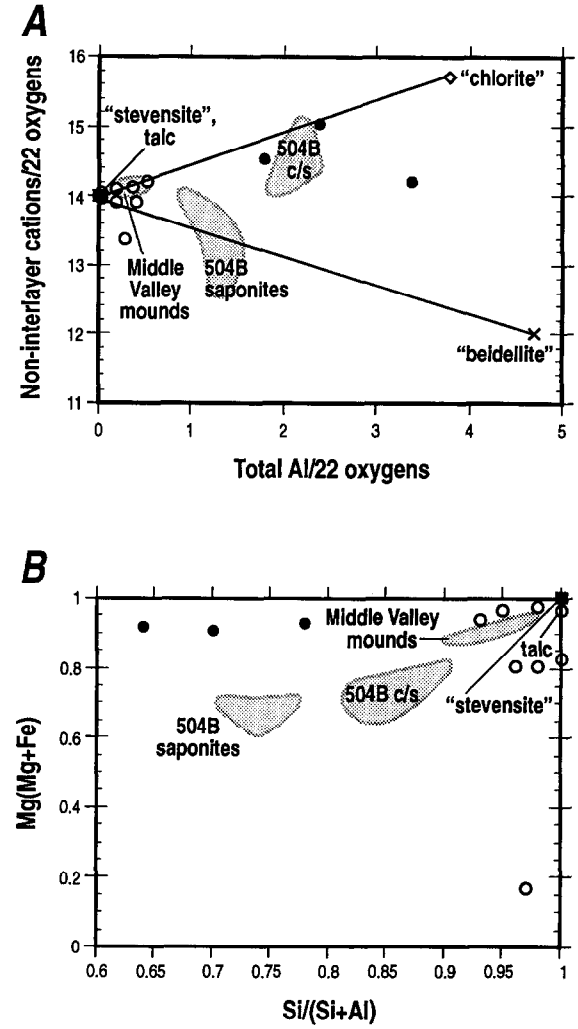


Fig. 6. Composition of layer-silicate minerals from Sea Cliff hydrothermal field. (A) Total Al versus total non-interlayer cations (recalculated on a 22 oxygen basis). (B) Si/(Si+Al) versus Mg/(Mg+Fe) ratios. Circles, smectites; dots, chlorite/smectite. Data from Deep Sea Drilling Project Site 504B from Shau and Peacor (1992); data from Middle Valley hydrothermal mounds and chimneys from Percival and Ames (1993).

Table 3
Chemical composition of basalt and altered rock from the Sea Cliff hydrothermal field

| | 767-3A | 767-3B | | 769-1A | 769-1B | | | 769-2A |
|---|---|---|---|---|---|---|---|---|
| | whole rock | whole rock | white clast | whole rock | whole rock | matrix | Dark clast | basalt |
| $SiO_2$ | 71.30 | 79.00 | 82.20[a] | 63.70 | 76.30 | 87.84[a] | 45.87[a] | 51.60 |
| $TiO_2$ | .03 | .03 | .01 | .04 | .04 | .03 | 1.43 | 1.40 |
| $Al_2O_3$ | 1.59 | 1.50 | 1.17 | 1.75 | 1.58 | .98 | 15.70 | 15.60 |
| FeO | 2.19 | 1.71 | .89 | 2.45 | 1.37 | 1.21 | 6.21 | 9.18 |
| MnO | .02 | .02 | .01 | .01 | .01 | .01 | .05 | .18 |
| MgO | 6.53 | 4.86 | 6.81 | .96 | 3.23 | 1.33 | 13.90 | 8.62 |
| CaO | .21 | .06 | .07 | .22 | .11 | .06 | 5.98 | 13.00 |
| $Na_2O$ | 1.00 | .71 | .66[a] | .64 | .47 | .36[a] | 1.89[a] | 2.55 |
| $K_2O$ | .30 | .25 | .26[a] | .20 | .19 | .14[a] | .17[a] | .13 |
| $P2O_5$ | .10 | .03 | .05 | .14 | .03 | .03 | .30 | .11 |
| SO3 | 4.72 | 3.97 | .12[a] | 13.56 | 5.97 | .37[a] | .17[a] | .17 |
| BaO | 4.80 | 3.24 | .06 | 8.49 | 7.37 | 0.00 | .12 | 0.01 |
| LOI | 6.80 | 6.10 | n.d. | 5.60 | 6.80 | n.d. | n.d. | .10 |
| Total | 99.59 | 101.48 | 92.31 | 97.76 | 103.47 | 92.36 | 91.79 | 102.65 |
| Ag | 5 | 4 | n.d. | 250 | 14 | 310 | 1 | 0 |
| As | 149 | n.d. | n.d. | 179 | n.d. | n.d. | n.d. | n.d. |
| Au | .628 | n.d. | n.d. | 1.605 | n.d. | n.d. | n.d. | n.d. |
| Be | 0 | .1 | .1 | .1 | .2 | .4 | 1.0 | .6 |
| Co | 6 | 3 | 4 | 7 | 3 | 6 | 71 | 35 |
| Cu | 840 | 630 | 310 | 1600 | 1600 | 3100 | 360 | 68 |
| Ni | 0 | 0 | 38 | 0 | 0 | 52 | 100 | 92 |
| Pb | 180 | n.d. | 92 | 1300 | 150 | 410 | 140 | 2 |
| Rb | n.d. | 6.0 | n.d. | n.d. | 5.2 | 3.7 | 4.3 | 1.4 |
| Sb | 7.6 | n.d. | n.d. | 25.1 | n.d. | n.d. | n.d. | n.d. |
| Se | 3.6 | n.d. | n.d. | 13.3 | n.d. | n.d. | n.d. | n.d. |
| Sn | 16 | n.d. | n.d. | 8 | n.d. | n.d. | n.d. | n.d. |
| Sr | 1200 | 600 | 660 | 990 | 840 | 260 | 120 | 120 |
| V | 45 | 30 | 27 | 67 | 49 | 51 | 240 | 230 |
| Yb | 0 | 0 | 0 | .4 | .1 | .2 | 2.5 | 2.3 |
| Zn | 350 | 260 | 210 | 5100 | 870 | 8400 | 1900 | 56 |
| Zr | n.d. | 5 | 2 | n.d. | 4 | 2 | 95 | 99 |

n.d. not determined
[a]Determined by electron microprobe on fused-glass bead prepared from separate subsample of material drilled from the same area of the rock as the major-element sample.

stant. Elements that are enriched relative to the starting basalt will plot above this line, and those that are depleted will plot below this line. Elements with the same degree of enrichment or depletion will plot along lines of constant slope passing through the origin (Grant, 1986).

The assumption that the unaltered basalt (sample 769-2) is a reasonable protolith for fragments in the hyaloclastite crust is supported by analyses of rare glassy clasts (Table 1) and by arguments implied by the data plotted in Fig. 7. The contents of elements generally assumed to be relatively immobile during hydrothermal alteration, including $Al_2O_3$, $TiO_2$, Ni, V, Yb, and Zr, are similar in the altered clast and the basalt. MgO and Rb are strongly enriched in the clast, whereas FeO, $Na_2O$, and CaO are depleted. In contrast, the whole-rock compositions of the crust and the matrix are inconsistent with relative immobility of trace elements. $SiO_2$ and Rb are enriched, and all other elements, except $K_2O$, are strongly depleted, in both the whole rock and matrix relative to basalt. The petrographic evidence clearly indicates addition of silica to

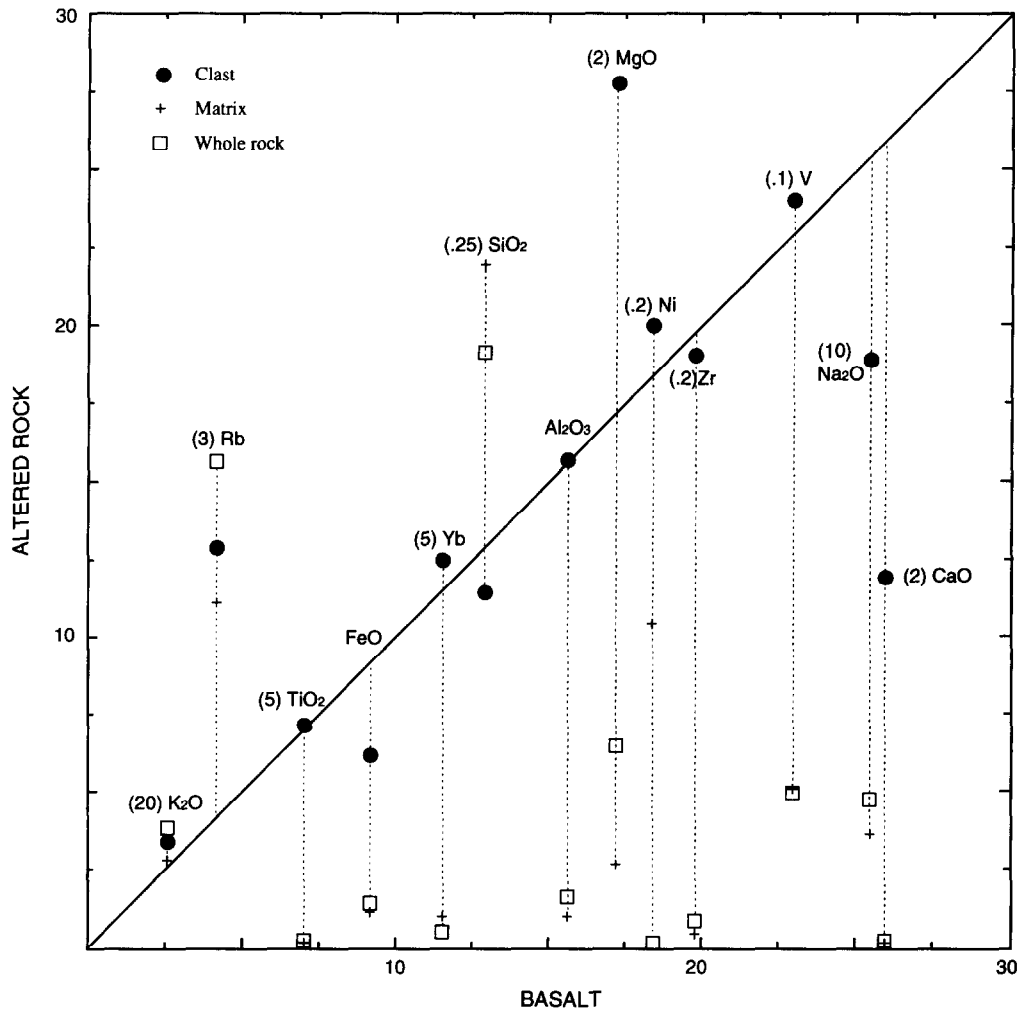


Fig. 7. Isocon plot (after Grant, 1986) showing enrichment and depletion relative to basalt for a dark clay altered clast (dots), the siliceous matrix (pluses), and whole-rock hyaloclastite crust (squares) from sample 769-1. Major-element contents in weight percent; minor-element contents in parts per million. Some elements are ratioed by factors listed in parentheses to reduce scale of plot and to avoid elements plotting on top of each other.

the rock, both by silicification of hyaloclastite fragments and by deposition in open space between fragments. If addition of silica were the only process affecting the crusts, whole-rock composition would show a constant depletion by dilution, and the elements that remained immobile would plot on a straight line passing through the origin. This behavior is clearly not seen. The chemical data support the petrographic observation of near-total silicification of many of the basaltic fragments and require that elements, including $Al_2O_3$, $TiO_2$, and Zr, have been removed from the fragments during silicification, even though many of these fragments retain a recognizable volcanic texture.

Comparison of the composition of a white silica and clay altered clast from sample 767-3 with the whole-rock composition of this crust shows similar results (Table 3). The altered clast and the whole rock are both highly siliceous and similar in composition, except for $SO_3$ enrichment in the whole rock, reflecting the presence of barite in the matrix of the sample.

Table 4
Isotopic composition of basalt and altered rock from the Sea Cliff hydrothermal field

| | $\delta^{18}O$ | $\delta^{34}S$ | | $^{87}Sr/^{86}Sr$ | $^{206}Pb/^{204}Pb$ | $^{207}Pb/^{204}Pb$ | $^{208}Pb/^{204}Pb$ |
|---|---|---|---|---|---|---|---|
| | | pyrite | barite | | | | |
| 767-3 | | | | | | | |
| Hyaloclastite | 22.1 | 2.2 | 18.7 | 0.70566 | 18.206 | 15.397 | 37.582 |
| White Clast | 20.0 | – | – | – | – | – | – |
| 769-1 | | | | | | | |
| Hyaloclastite | 22.9 | 1.1 | 21.6 | 0.70528 | 18.213 | 15.426 | 37.590 |
| Matrix | 22.1 | – | – | – | – | – | – |
| Dark clast | 6.1 | – | – | – | – | – | – |
| Sulfide clast | – | 3.4 | – | – | 18.294 | 15.504 | 37.875 |
| 769-2 | | | | | | | |
| Basalt | 5.9 | – | – | 0.70238 | 18.300 | 15.484 | 37.774 |
| 769-3 | | | | | | | |
| Hyaloclastite | – | 3.7 | – | – | – | – | – |
| 769-4 | | | | | | | |
| Hyaloclastite | – | 2.4 | 20.2 | – | – | – | – |

## 8. Isotopic data

The unaltered-basalt sample (769-2) has oxygen-, strontium-, and lead-isotopic compositions typical Gorda Ridge basalt (Table 4). The lead-isotope compositions of the hyaloclastite crusts are similar to those of the basalt (Fig. 8). The strontium-isotopic compositions of the hyaloclastite crusts, however, are significantly more radiogenic ($^{87}Sr/^{86}Sr = 0.7054 \pm 2$ versus 0.7024, Fig. 9). The two whole-rock oxygen-isotopic compositions of the hyaloclastite crusts are quite heavy relative to unaltered basalt, with $\delta^{18}O$ values of 22.1‰ and 22.9‰. A highly silicified clast from sample 767-3 has a $\delta^{18}O$ value of 20.0‰, whereas a dark, less altered clast from sample 769-1 has a $\delta^{18}O$ value of 6.1‰. $\delta^{34}S$ values of disseminated sulfide minerals in the hyaloclastites and a massive sulfide clast that was drilled from sample 769-1 range from 1.1‰ to 3.7‰, typical for hydrothermal sulfides formed on sediment-free spreading centers (Arnold and Sheppard, 1981; Styrt et al., 1981; Zierenberg et al., 1984; Woodruff and Shanks, 1988). The lead-isotopic composition of the massive sulfide clast is similar to that of Gorda Ridge basalt (Fig. 8). $\delta^{34}S$ values of barite in the crusts range from 18.7‰ to 21.6‰, similar to or slightly lower than that of seawater sulfate (21‰; Rees et al., 1978).

## 9. Discussion

### 9.1. Magnesium metasomatism and silicification

Extensive alteration led to near-complete silicification of most basaltic fragments contained in the hydrothermal crust. Some fragments, however, are not completely altered, and careful examination of these fragments reveals the sequence of alteration reactions that leads to silicification. Many fragments have cores of Mg-rich smectite mantled by silicified rims. Less commonly, basaltic cores with remnant microphenocrysts are preserved as the innermost zone of Mg-rich smectite or chlorite/smectite replacement, especially in larger fragments. These petrographic relationships reveal that the first step in alteration is Mg metasomatism of the basaltic glass. Analysis of a chlorite/smectite-altered clast from sample 769-1 shows a near doubling of the Mg content relative to unaltered basalt, accompanied by losses of Na, Ca, and Fe and minor depletion of Si (Fig. 7). The alteration is directly analogous to that produced experimentally by high-temperature alteration of basalt by seawater (Bischoff and Dickson, 1975; Seyfried and Bischoff, 1977). In the experimental alteration of basalt, Mg addition occurs by incorporation of seawater-derived Mg into the hydroxyl layer of smectite, with a resulting release of hydrogen ions, as shown in the generalized saponite-precipitation reaction:

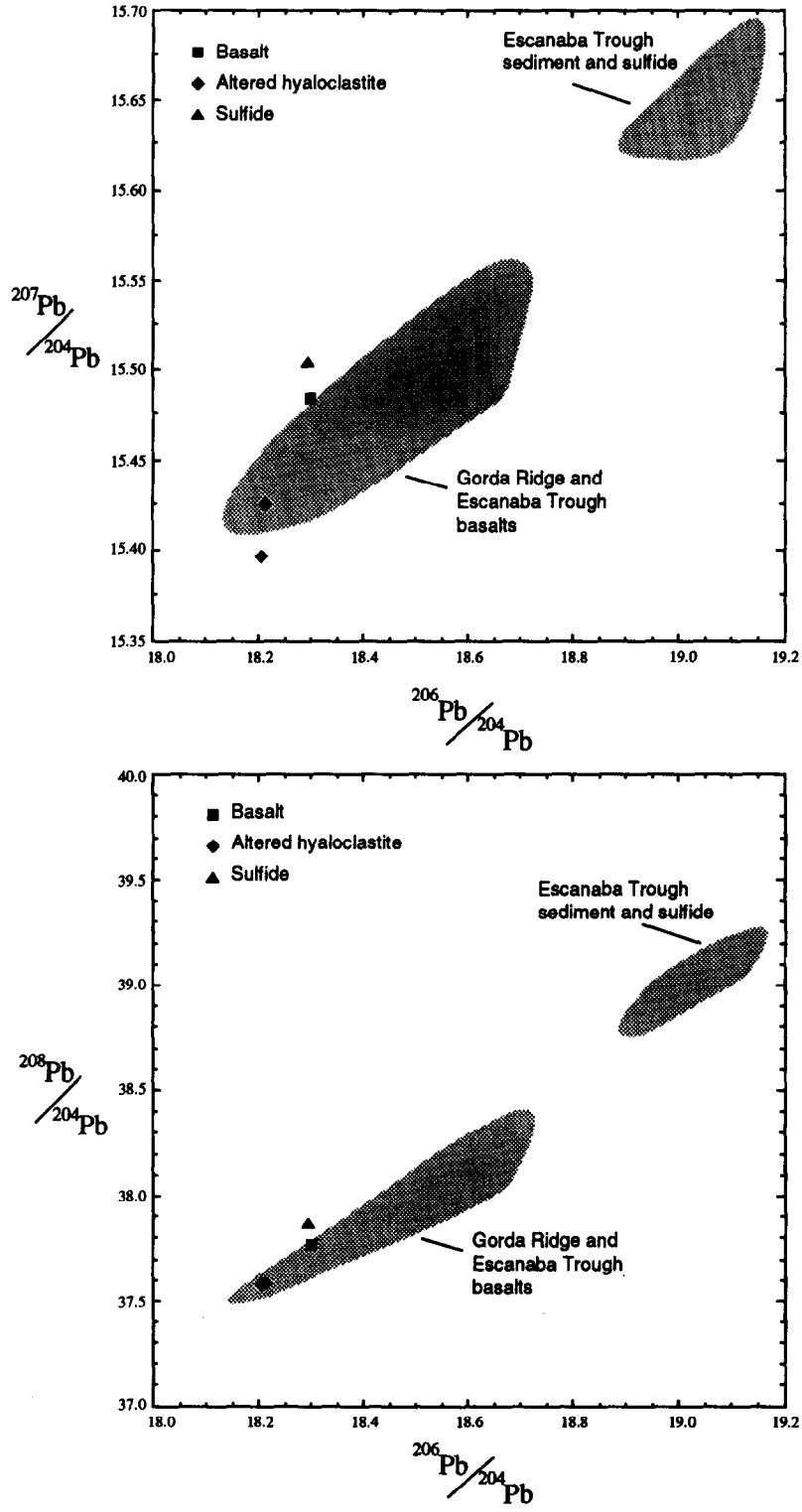


Fig. 8. Lead-isotopic ratios of basalt (squares), altered hyaloclastite (diamonds), and massive sulfide fragment (triangles) from altered hyaloclastite crusts. Shaded areas for Gorda Ridge and Escanaba Trough basalts, sulfides, and sediment from Church and Tatsumoto (1975), White et al. (1987), and Zierenberg et al. (1993). Symbol size is approximately equal to 0.1% uncertainty.

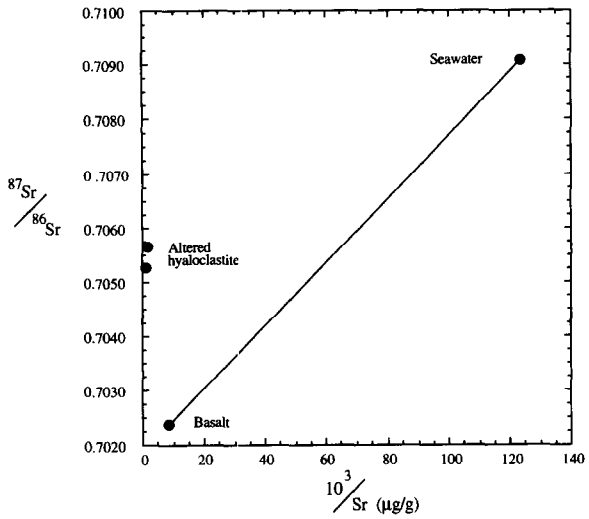


Fig. 9. Strontium-isotopic ratio versus inverse Sr content for basalt and altered hyaloclastite from the Sea Cliff hydrothermal field. Altered hyaloclastite samples have strontium-isotopic compositions intermediate between those of seawater and basalt but do not plot near simple two-component mixing line, owing to high Sr content of crust, which is mainly contained in hydrothermally precipitated barite.

$$3Mg^{+2} + 4SiO_2 + 4H_2O = Mg_3Si_4O_{10}(OH)_2 + 6H^+ \quad (1)$$

The production of hydrogen ions allows hydrolytic alteration of the basalt, releasing cations to the hydrothermal solution. Basaltic glass reacted more rapidly than crystalline basalt in the experiments, and when seawater-to-rock ratios were high enough that the amount of Mg does not limit the reaction, the basaltic glass was completely altered to Mg-rich smectite (Seyfried and Bischoff, 1979). Smectite produced by rapid alteration of basaltic glass is less well crystallized than smectite formed by alteration of diabase (Seyfried and Bischoff, 1979).

Although the experimental alteration of basalt at high water–rock ratios results in leaching of metals, alkalis, and alkaline earths from the basalt, most of the aluminum in the basalt is apparently retained in the chlorite/smectite alteration products (Seyfried and Bischoff, 1981). In contrast, petrographic evidence that shows a basaltic texture continuing from smectite-altered cores of clasts to silicified rims, as well as the composition of the white clast from sample 767-3, requires removal of aluminum and titanium, elements generally considered highly immobile. Aluminum solubility increases at low pH (Palmer and Wesolowski, 1992); however, Al contents in the basalt–seawater experimental solutions show that aluminum is sparingly soluble under most seafloor hydrothermal conditions. The strong depletion of aluminum and other relatively insoluble cations observed in Gorda Ridge hyaloclastites requires an extensive flow of hydrothermally altered seawater through the rocks. Hydrothermal alteration of fresh basaltic glass exposed to seawater during volcanic eruptions appears to result in more efficient solubilization of aluminum than that observed for deeper circulating hydrothermal fluids (Resing et al., 1992, 1993).

Although Mg metasomatism caused by basalt–seawater interaction at high water–rock ratios is clearly required to account for the extensive leaching of immobile elements from basaltic glass, the conditions of alteration are less certain. Isotopic data on the alteration products provide some constraints on the process. The Mg-enriched dark clast from sample 769-1 has a $\delta^{18}O$ value of 6.1‰. Extensive recrystallization of this clast to chlorite/smectite suggests that oxygen-isotopic compositions should approach equilibrium with the altering hydrothermal fluid. $\delta^{18}O$ values of hydrothermal fluids in ridge-crest hydrothermal systems generally range from 0‰ to 2‰; the high water–rock ratios indicated for Gorda Ridge samples by the Mg enrichment indicate mixing with relatively unaltered seawater, and so $\delta^{18}O$ values of the hydrothermal fluid were probably close to 0‰. Assuming a $\delta^{18}O$ value of 0‰ for the hydrothermal fluid, we can calculate an approximate temperature of formation of the smectite, using the fractionation equation of Yeh and Savin (1977). The calculated temperature of 220°C is close to the maximum measured temperature of 247°C in the adjacent vent field (Rona et al., 1990). The lower temperature is consistent with cooling by entrainment of seawater into the hydrothermal-discharge zone. These temperatures are also consistent with the crystallization temperature of chlorite/smectite in basalts altered in active, subaerial geothermal systems (Schiffman and Fridleifsson, 1991). Alternatively, we could assume that the smectite formed at 247°C, and calculate the isotopic composition of a hydrothermal fluid in equilibrium with smectite at the temperature of the active vents. The resulting $\delta^{18}O$ value of the fluid is 1.1‰, in

the middle of the range of measured seafloor-vent compositions.

The formation temperatures of the siliceous clasts and the bulk hyaloclastite crust can be estimated by again assuming an hydrothermal fluid with a near-seawater oxygen-isotopic composition and then calculating the fractionation, assuming that the samples are composed of amorphous silica. Using the fractionation equation of Kita et al. (1985) and the $\delta^{18}O$ values listed in Table 4, we estimate depositional temperatures in the range 85°–110°C. These low temperatures are consistent with the observation that amorphous silica is dominant in the samples, accompanied by lesser amounts of chalcedony and smectite, as opposed to well-crystallized quartz.

The abundance of amorphous silica in the samples requires that the concentration of dissolved silica in the altering hydrothermal fluid was well in excess of saturation values for quartz (Fournier, 1985). The high degree of supersaturation with respect to quartz may have been due to conductive cooling of a hydrothermal fluid that equilibrated with quartz in the subsurface at a temperature above 225°C (Fournier, 1985; Janecky and Seyfried, 1984), within the range of vent temperatures measured at this site (Rona et al., 1990). A more plausible explanation, however, consistent with petrographic observations is that the fluid was buffered to high silica activity by interaction with highly reactive basaltic glass, resulting in silica concentrations in the range necessary for precipitation of amorphous silica (Fournier, 1985).

Strontium is highly enriched in the altered hyaloclastite because of incorporation (in concentrations as high as 6 wt% SrO) in barite. The strontium-isotopic composition helps constrain the origin of the altering fluids. The Sr-isotopic composition of the hyaloclastites is intermediate between that of the two major strontium reservoirs in the system, basalt and seawater (Fig. 9), but could not result from a simple two-component mixing (Faure, 1977). The high strontium content in the samples also precludes simple addition of seawater strontium (via barite precipitation) to the strontium contained in the original basaltic clast, because isotopic mass balance indicates that the crust should have an $^{87}Sr/^{86}Sr$ ratio of 0.7084 if seawater-derived strontium were the only source of strontium in the barite. Although basalt- and seawater-derived strontium are likely present in approximately equal amounts in the hydrothermal barite, they must have been buffered at this ratio in the hydrothermal fluid. Similarity of the $^{87}Sr/^{86}Sr$ ratio in two samples collected from different parts of the hydrothermal field suggests a fairly homogeneous strontium-isotopic composition of the hydrothermal fluid, although the hydrothermal vents at this site have not yet been sampled. Hydrothermal fluids from sediment-free spreading centers have $^{87}Sr/^{86}Sr$ ratios that range from 0.7029 to 0.7047. The slightly higher ratios in the altered hyaloclastite crusts could have resulted from higher water–rock ratios in the hydrothermal-reaction zone deep beneath this site or, more likely, mixing of some unaltered seawater with hydrothermal fluid in the shallow subsurface. Because end-member hydrothermal fluids have very low concentrations of both magnesium and sulfate, the abundance of Mg-rich smectite and barite in the crusts indicates that unaltered seawater must mix into the alteration zone.

An alternative source of radiogenic strontium in the crust should also be considered. Because the Sea Cliff hydrothermal field lies several kilometers off axis, the basaltic rocks in the high-temperature reaction zone may have been previously altered by pervasive hydrothermal circulation at lower temperature. Studies of the Cyprus ophiolite show that the sheeted dike complex and the uppermost plutonic rocks were pervasively altered and have $^{87}Sr/^{86}Sr$ ratios that cluster around 0.7054 (Bickle and Teagle, 1992), similar to those in the hyaloclastite crusts. A high-temperature hydrothermal-circulation cell that developed off axis in previously altered rocks could therefore be expected to have an $^{87}Sr/^{86}Sr$ ratio in this range.

Because the Sea Cliff hydrothermal field is off axis, we need to consider whether leaching of detrital sediment contributed to the hydrothermal system, possibly affecting the strontium-isotopic compositions of the samples. Hydrothermal fluids sampled on sediment-covered spreading centers in the Guaymas Basin and Escanaba Trough contain radiogenic strontium derived from the sediment cover (Palmer and Edmond, 1989). The involvement of sediment in the Escanaba Trough system also is clearly indicated by the lead-isotopic composition of hydrothermal precipitates (Fig. 8; Zierenberg et al., 1993). Lead-isotopic compositions of the altered hyaloclastite crusts and a fragment of massive sulfide from the crusts are similar to those of unaltered basalt from the vent field and those of previously ana-

lyzed Gorda Ridge basalts, indicating that sediment-derived lead is not an abundant component of this hydrothermal system. Therefore, strontium-isotopic compositions also were probably not affected by leaching of sediment.

### 9.2. Tectonics and geochemical setting of hydrothermal alteration within the Sea Cliff hydrothermal field

Although the Sea Cliff hydrothermal field is poorly explored and poorly sampled, several features differentiate it from most other known seafloor hydrothermal sites. The active venting is not occurring in the neovolcanic zone but about 2.6 km off axis. The largest known seafloor hydrothermal sites, including the TAG site on the Mid-Atlantic Ridge (Thompson et al., 1988) and the Endeavour Main Field on the Juan de Fuca Ridge (Delaney et al., 1992), are also off axis, but both of these deposits are situated at the base of large normal faults that define the main grabens of mature spreading ridges (Franklin, 1986). The Sea Cliff hydrothermal field is also associated with the innermost major normal fault defining the axial valley, but in contrast to other known active seafloor hydrothermal systems, it is developed in the fault talus at an elevation approximately 300 m above the floor of the axial valley. Its position at the south end of an elevated ridge may be controlled by enhanced fracture permeability at the intersection of two structural trends (Rona and Clague, 1989). Development of the system in fault talus and hyaloclastite is further evidence that the shallow subsurface of the deposit is highly permeable and thus that mixing of infiltrating cold seawater and hydrothermal fluid in the shallow subsurface is probably enhanced in this deposit relative to on-axis hydrothermal systems developed in basaltic sheet flows.

Extensive areas of the Sea Cliff hydrothermal field are apparently capped by hydrothermal crusts. The recovered samples of these crusts are hyaloclastite breccias that have been highly altered by initial Mg-metasomatism followed by silicification. Geochemical and isotopic constraints on the alteration process indicate that the altering fluids were mixtures of high-temperature hydrothermal fluid and cold seawater and that the near-surface alteration occurred at relatively low temperatures in what was apparently a long lived, diffuse flow field capable of supporting vent-specific biologic communities. The altered hyaloclastite crust, which is extensively cemented by amorphous silica and barite, may have formed a relatively impermeable cap on the hydrothermal system, allowing more extensive precipitation of sulfide in the permeable talus and hyaloclastite. This capping may have suppressed development of chimneys that allow venting of high-temperature hydrothermal fluid directly into the water column, with subsequent dispersal of base-metal sulfide minerals in black-smoker plumes. A similar setting has been described for the Galápagos Fossil Hydrothermal Field, where Mg metasomatism related to subseafloor mixing of hydrothermal fluid and seawater is an important process in the alteration of the volcanic host rocks (Ridley et al., 1994). Recent drilling on the TAG hydrothermal mound reveals extensive deposition of anhydrite beneath the surface of the mound due to mixing of cold seawater with hydrothermal fluid circulating within the mound (Herzig et al., 1995). Silicified basalt fragments pass downward to chloritized basalt fragments below the TAG sulfide mound (Herzig et al., 1995). Environments that allow extensive subsurface mixing may be more favorable for the formation of large metal deposits than on-axis sites, and are comparable to the environment of some ophiolite-hosted massive sulfide deposits.

### 9.3. Comparison to ophiolite-hosted sulfide deposits

The geologic setting, mechanism, and extent of hydrothermal alteration of the hyaloclastite crust from the Sea Cliff hydrothermal field are analogous to those of the massive sulfide mineralization at the Turner-Albright deposit in southern Oregon, and is similar to alteration sequences described from other massive sulfide deposits. The Turner-Albright deposit is in Late Jurassic rocks of the Josephine ophiolite, which formed in a backarc setting (Harper, 1984). The Turner-Albright deposit has been interpreted to have formed near a backarc spreading center (Strickler, 1986; Kuhns and Baitis, 1987; Zierenberg et al., 1988).

The least altered host rocks associated with Turner-Albright mineralization are sparsely mineralized chloritic breccias. Textures of the breccia fragments include finely banded clasts interpreted as devitrified basaltic glass (Fig. 5e, 5f) with some fragments retaining chromium spinel microphenocrysts and phenocrysts and microlites of olivine and plagioclase pseudomorphi-

cally replaced by chlorite and quartz, respectively. Where mineralization and alteration are more intense, the proportion of quartz in the alteration minerals increases. Rocks at intermediate stages of alteration contain the mineral assemblage quartz–chlorite–sericite. The most highly altered rocks in semimassive to massive sulfide are completely replaced by quartz and sulfide. The only vestige of the original volcanic heritage in these silicified rocks is the presence of chromium spinel microphenocrysts. These extensively silicified basalts have typically been misinterpreted as exhalative cherts that were codeposited with the massive sulfide mineralization. Only a part of the mineralization at the Turner-Albright deposit formed on the paleoseafloor by true exhalative mineralization; most formed by both cementation and replacement of a thick sequence of basaltic hyaloclastites in the shallow subsurface, below the vents that formed the thinner massive sulfide capping to the deposit (Strickler, 1986; Zierenberg et al., 1988). Initial alteration of basalt to chlorite occurred at higher temperatures (250–350°C), but the quartz in highly silicified fragments has an oxygen-isotopic composition indicative of equilibration with a seawater-like fluid at temperatures near 200°C (Zierenberg et al., 1988). Some silicified fragments have textures indicative of deposition as amorphous silica.

The major difference in the alteration of the hyaloclastite at the Turner-Albright deposit compared to the Sea Cliff hydrothermal field is that the initial high-temperature stage of alteration of basaltic glass at Turner-Albright is to an Fe-rich chlorite, whereas within the Sea Cliff hydrothermal field the equivalent alteration is to Mg-rich smectite. The chlorite altered rocks from Turner-Albright are preserved only in the deeper parts of the hydrothermal-alteration zone; rocks closer to the paleoseafloor are completely silicified. Zierenberg et al. (1988) attributed the initial alteration to Fe-rich, Mg-depleted, high-temperature hydrothermal fluid similar to the fluids produced by experimental basalt–seawater interaction (Seyfried and Bischoff, 1981) or sampled at hydrothermal vents on active spreading centers (Von Damm et al., 1985).

In contrast, initial alteration of hyaloclastite within the Sea Cliff hydrothermal field occurred on the seafloor in a mixing zone between high-temperature, Mg-depleted hydrothermal fluid and cold seawater that provided the magnesium for the formation of smectite. Both systems produced to the same type of alteration: complete replacement of basaltic-glass fragments by silica with the removal of all cations, including aluminum and titanium. The high silica concentrations required for deposition of amorphous silica were established by alteration of highly reactive basaltic glass. The extensive alteration and final deposition of quartz and (or) amorphous silica at fairly low temperature indicates a long-lived, diffuse-flow regime more akin to white smokers and tubeworm fields than to the black smokers typically associated with massive sulfide deposition. Lydon and Galley (1986) described a nearly identical alteration sequence from the Mathiati deposit, Cyprus, which displays extensive silicification of basalt in the alteration zone underlying the massive sulfide ore.

On-axis hydrothermal deposits are characterized by black-smoker chimneys. The amount of metal precipitated in these chimneys is small relative to that transported to the site by the hydrothermal fluid. Most of the dissolved-metal load is precipitated by rapid cooling during mixing in the buoyant plumes that give rise to the name 'black smokers'. These plumes typically rise several hundred meters above the seafloor and are carried off axis by the prevailing currents. In present-day, well-mixed, oxygenated oceans, the fate of the sulfide particulates in the plume is oxidation and dispersal from the site of hydrothermal discharge. The local hydrology at the discharge site can strongly affect the resulting mineral deposit. Whereas on-axis hydrothermal systems typically vent from relatively unfractured basalt, hydrothermal systems along rift-bounding normal faults are typically developed in tectonic breccias and fault talus (e.g., Ridley et al., 1994). This setting is more conducive to diffuse flow, which will allow more time for conductive cooling, increased mixing with cold seawater, and enhanced reaction of hydrothermal fluid with the brecciated rock. All of these processes will favor metal deposition both immediately below and on the seafloor, leading to the decreasing loss of metallic ions to the water column that is typical of focused high-temperature discharge. Hydration of the basaltic breccia and cementation by precipitated silica can further restrict flow and potentially can cap the hydrothermal system. If water depths are sufficiently shallow or fluid temperatures sufficiently high, the silica cap can be breached by hydrothermal explosions,

as proposed for the Mathiati deposit by Lydon and Galley (1986).

## 10. Conclusions

The extensive hydrothermal crusts in the Sea Cliff hydrothermal field formed from basaltic hyaloclastite that has been highly altered and cemented by silica. The initial stage of alteration was Mg metasomatism of basaltic glass at temperatures near 250°C. High water–rock ratios are required to explain the extent of alteration, which resulted in removal of most cations from the basalt, including sparingly soluble aluminum and titanium. The reactivity of the basaltic glass resulted in high silica activity, which enhanced both silicification of the basalt and precipitation of abundant amorphous silica in the matrix. Silicification of clasts and amorphous-silica cementation proceeded to relatively low temperatures (85–110°C). The abundance of Mg-rich smectite and chlorite/smectite, the precipitation of barite with seawater-derived sulfate, and the strontium-isotopic compositions between those of basalt and seawater indicate that mixing of hydrothermal fluid with seawater in the shallow subsurface is an important process in the alteration of the crusts. Lead isotopic compositions indicate that sedimentary rocks are not a significant component in this hydrothermal system, even though hydrothermal circulation developed in an off-axis setting.

The setting of the Sea Cliff hydrothermal field is similar to that of many ophiolite-hosted massive sulfide deposits. Diffuse hydrothermal discharge and subseafloor cooling and mixing may result in more efficient deposition of metallic sulfides and increase the chances that a hydrothermal system will develop an economic ore deposit. Extensive alteration and replacement of basalt is a fundamental process in the formation of volcanogenic massive sulfide deposits, and a large part of many of these so-called exhalative deposits may form below the seafloor because of the mixing of hydrothermal fluids with cold seawater.

## Acknowledgements

We gratefully acknowledge the cooperation of the U.S. Navy Submarine Development Group One, and especially the dedicated efforts of the crew of DSV *Sea Cliff*, for their support of the dive program and collection of samples, often under adverse weather conditions. McClain and Schiffman acknowledge support under Contract 63-630-8804 from Oregon Dept. of Geology and Mineral Industries and the Gorda Ridge Technical Task Force. Reviews by J. Hein, I. Ridley, H. Furnes, C. Mevel, and B. Peucker-Ehrenbrink improved the manuscript.

## References

Arnold, M. and Sheppard, M.F., 1981. East Pacific Rise at latitude 21°N: isotopic composition and origin of the hydrothermal sulfur. Earth Planet. Sci. Lett., 56: 148–156.

Atwater, T. and Mudie, J.D., 1973. Detailed near-bottom geophysical study of the Gorda Ridge. J. Geophys. Res., 78: 8665–8686.

Baker, E.T., Massoth, G.J., Collier, R.W., et al., 1987. Evidence for high-temperature hydrothermal venting on the Gorda Ridge, northeast Pacific Ocean. Deep Sea Res., 34: 1461–1476.

Bickle, M.J. and Teagle, D.A.H., 1992. Strontium alteration in the Troodos ophiolite: implications for fluid fluxes and geochemical transport in mid-ocean ridge hydrothermal systems. Earth Planet. Sci. Lett., 113: 219–237.

Bischoff, J.L. and Dickson, F.W., 1975. Seawater–basalt interaction at 200°C and 500 bars: implications for origin of sea-floor heavy-metal deposits and regulation of seawater chemistry. Earth Planet. Sci. Lett., 25: 385–397.

Breit, G.N., Simmons, E.G. and Goldhaber, M.B., 1985. Dissolution of barite for the analysis of strontium isotopes and other chemical and isotopic variations using aqueous sodium carbonate. Chem. Geol., 52: 333–336.

Brown, R.W., 1977. A sample fusion technique for whole rock analysis with the electron microprobe. Geochim. Cosmochim. Acta, 41: 435–438.

Canfield, D.E., Raiswell, R., Westrich, J.T., Reaves, C.M. and Berner, R.A., 1986. The use of chromium reduction in the analysis of reduced inorganic sulfur in sediments and shales. Chem. Geol., 54: 149–155.

Church, S.E. and Tatsumoto, M., 1975. Lead isotope relations in oceanic ridge basalts from the Juan de Fuca–Gorda area, N.E. Pacific Ocean. Contrib. Mineral. Petrol., 53: 253–279.

Clague, D.A. and Holmes, M.L., 1987. Geology, petrology, and mineral potential of the Gorda Ridge. In: D.W. Scholl, A. Grantz and J.G. Vedder (Editors), Geology and Resource Potential of the Continental Margin of Western North America and Adjacent Ocean Basins—Beaufort Sea to Baja California. Circum-Pacific Council for Energy and Mineral Resources, Earth Science Series. Houston, TX, pp. 563–580.

Clague, D.A. and Rona, P.A., 1990. Geology of the GR 14 site on northern Gorda Ridge. In: G.R. McMurray (Editor), Gorda Ridge: A Seafloor Spreading Center in the United States' Exclusive Economic Zone. Springer-Verlag, New York, pp. 31–50.

Collier, R.W. and Baker, E.T., 1990. Hydrography and geochemistry of northern Gorda Ridge, In: G.R. McMurray (Editor), Gorda Ridge: A Seafloor Spreading Center in the United States' Exclusive Economic Zone. Springer-Verlag, New York, pp. 21–29.

Collier, R.W., Holbrook, S.H. and Robbins, J.M., 1986. Studies of trace metals and active hydrothermal venting on the Gorda Ridge. Ore. Dept. Geol. Miner. Ind. Open-File Rep., O-86-13, 36 pp.

Delaney, J.R., Robigou, V., McDuff, R. and Tivey, M.K., 1992. Geology of a vigorous hydrothermal system on the Endeavour Segment, Juan de Fuca Ridge. J. Geophys. Res., 97: 19,663-19,682.

Embley, R.W., Jonasson, I.R., Perfit, M.R., Franklin, J.M., Tivey, M.A., Malahoff, A., Smith, M.F. and Francis, T.J.G., 1988. Submersible investigation of an extinct hydrothermal system on the Galapagos Ridge: sulfide mounds, stockwork zone and differentiated lavas. Can. Mineral., 26: 517–540.

Faure, G., 1977. Principles of Isotope Geology. John Wiley and Sons, New York, 464 pp.

Fisk, M.R. and Howard, K.J., 1989. Mineral deposits recovered from northern Gorda Ridge: mineralogy and chemistry. Ore. Dept. Geol. Miner. Ind. Open-File Rep., O-89-09, 26 pp.

Fournier, R.O., 1985. The behavior of silica in hydrothermal systems. Rev. Econ. Geol., 2: 45–61.

Franklin, J.A., 1986. Volcanic-associated massive sulphide deposits—an update. In: C.J. Andrew, R.W.A. Crowe, S. Finlay, W.M. Pennell, and J.F. Pyne (Editors), Geology and Genesis of Mineral Deposits in Ireland. Irish Assoc. for Econ. Geol., Dublin, pp. 49–70.

Grant, J.A., 1986. The isocon diagram—a simple solution to Gresens equation for metasomatic alteration. Econ. Geol., 81: 1976–1982.

Harper, G.D., 1984. The Josephine ophiolite, northwestern California. Geol. Soc. Am. Bull., 95: 1009–1026.

Herzig, P.M., Humphris, S.E. and the Leg 158 Shipboard Scientific Party, 1995. Ocean Drilling Program reveals the subsurface nature of the TAG hydrothermal mound. InterRidge News, 4 (1): 11–14.

Janecky, D.R. and Seyfried, W.E., Jr., 1984. Formation of massive sulfide deposits on oceanic ridge crests: incremental reaction models for mixing between hydrothermal solutions and seawater. Geochim. Cosmochim. Acta, 48: 2723–2738.

Kita, I., Taguchi, S. and Matsubaya, O., 1985. Oxygen isotope fractionation between amorphous silica and water at 34–93°C. Nature, 314: 63–64.

Kuhns, R.J. and Baitis, H.W., 1987. Preliminary study of the Turner-Albright Zn–Cu–Ag–Au–Co massive sulfide deposit, Josephine County, Oregon. Econ. Geol., 81: 1362–1676.

Larocque, A.C., Jonasson, I.R. and LeCheminant, G.M., 1989. Zonation of secondary minerals in hydrothermally altered seafloor lavas from the Galapagos Rift. In: Current Research, Part F, Geol. Surv. Can., 89-1F: 9–15.

Lydon, J.W. and Galley, A., 1986. The chemical and mineralogical zonation of Mathiati alteration pipe, Cyprus, and its genetic significance. In: M.J. Gallagher, R.A. Ixer, C.R. Neary and H.M. Prichard (Editors), Metallogeny of Basic and Ultrabasic Rocks. Inst. of Mining and Metallurgy, London, pp. 49–71.

Macdonald, K.C., Scheirer, D.S. and Carbotte, S.M., 1991. Mid-ocean ridges: discontinuities, segments and giant cracks. Science, 253: 986–994.

McClain, J.S. and Schiffman, P., 1989. Submersible observations and bottom-sample analyses of the Sea Cliff hydrothermal field, Gorda Ridge. Ore. Dept. Geol. Min. Ind., Open-File Rep., O-89-08, 27 pp.

Palmer, M.R. and Edmond, J.M., 1989. The strontium isotope budget of the modern ocean. Earth Planet. Sci. Lett., 92: 11–26.

Palmer, D.A. and Wesolowski, D.J., 1992. Aluminum speciation and equilibria in aqueous solution, II. The solubility of gibbsite in acidic sodium chloride solutions from 30 to 70°C. Geochim. Cosmochim. Acta, 56: 1093–1111.

Percival, J.B. and Ames, D.E., 1993. Clay mineralogy of active hydrothermal chimneys and an associated mound, Middle Valley, northern Juan De Fuca Ridge. Can. Mineral., 31: 957–971.

Rees, C.E., 1978. Sulphur isotopic measurements using $SO_2$ and $SF_6$. Geochim. Cosmochim. Acta, 42: 383–390.

Rees, C.E., Jenkins, W.J. and Monster, J., 1978. The sulfur isotopic composition of ocean water sulfate. Geochim. Cosmochim. Acta, 42: 377–381.

Resing, J.A., Sansone, F.J., Wheat, C.G., Measures, C.I., McMurtry, G.M., Sedwick, P.N. and Massoth, G.J., 1992. The extraction of aluminum from hot rock: the elemental signature of an eruption vs. classical hydrothermal system. Trans. Am. Geophys. Union, EOS, 73: 254.

Resing, J.A., Sansone, F.J., Wheat, C.G., Massoth, G.J. and Baker, E., 1993. The water column Al signature at the 1993 coaxial eruption site on the Juan de Fuca ridge. Trans. Am. Geophys. Union, EOS, 74: 620.

Riddihough, R.P., 1980. Gorda Plate motions from magnetic anomaly analysis. Earth Planet. Sci. Lett., 51: 163–170.

Ridley, W.I., Perfit, M.R., Jonasson, I.R. and Smith, M.F., 1994. Hydrothermal alteration in oceanic ridge volcanics: A detailed study at the Galapagos Fossil Hydrothermal Field. Geochim. Cosmochim. Acta, 58: 2477–2494.

Rona, P.A. and Clague, D.A., 1989. Geologic controls of hydrothermal discharge on the northern Gorda Ridge. Geology, 17: 1097–1101.

Rona, P.A., Denlinger, R.P., Fisk, M.R., Howard, K.J., Taghon, G.L., Klitgord, K.D., McClain, J.S., McMurray, G.R. and Wiltshire, J.C., 1990. Major off-axis hydrothermal activity on the northern Gorda Ridge. Geology, 18: 493–496.

Schiffman, P. and Fridleifsson, G.O., 1991. The smectite to chlorite transition in drillhole NJ-15, Nesjavellir geothermal field, Iceland: XRD, BSE, and electron microprobe investigations. J. Metamorph. Geol., 9: 679–696.

Schiffman, P., Zierenberg, R.A. and McClain, J.S., 1989. Hydrothermal crusts from the Sea Cliff Hydrothermal Field Gorda Ridge: a modern analogue of silicified zones found within ophiolitic massive sulfide deposits. Trans. Am. Geophys. Union, EOS, 70: 1397.

Seyfried, W.E., Jr. and Bischoff, J.L., 1977. Hydrothermal transport of heavy metals by seawater: the role of seawater:basalt ratio. Earth Planet. Sci. Lett., 34: 71–77.

Seyfried, W.E., Jr. and Bischoff, J.L., 1979. Low temperature basalt alteration by seawater: an experimental study at 70°C and 150°C. Geochim. Cosmochim. Acta, 43: 1937–1947.

Seyfried, W.E., Jr. and Bischoff, J.L., 1981. Experimental seawater–basalt interaction at 300°C, 500 bars, chemical exchange, secondary mineral formation and implications for the transport of heavy metals. Geochim. Cosmochim. Acta, 45: 135–149.

Shau, Y.-H. and Peacor, D.R., 1992. Phyllosilicates in hydrothermally altered basalts from DSDP Hole 540B, Leg 83—a TEM and AEM study. Contrib. Mineral. Petrol., 112: 119–133.

Strickler, M.D., 1986. Geological setting of the Turner-Albright massive sulfide deposit, Josephine County, Oregon. Ore. Geol., 48: 115–122.

Styrt, M.M., Brackmann, A.J., Holland, H.D., Clark, B.C., Pisutha-Arnond, V., Eldridge, C.S. and Ohmoto, H., 1981. The mineralogy and the isotopic composition of sulphur in hydrothermal sulfide/sulfate deposits on the East Pacific Rise, 21°N latitude. Earth Planet. Sci. Lett., 53: 382–390.

Thompson, G., Humphris, S.E., Schroeder, B., Sulanowska, M. and Rona, P.A., 1988. Active vents and massive sulfides at 26°N (TAG) and 23°N (Snakepit) on the Mid-Atlantic Ridge. Can. Mineral., 26: 697–711.

Von Damm, K.L., Edmond, J.M., Grant, B., Measures, C.I., Walden, B. and Weiss, R.F., 1985. Chemistry of submarine hydrothermal solutions at 21°N, East Pacific Rise. Geochim. Cosmochim. Acta, 49: 2197–2221.

White, W.M., Hofmann, A.W. and Puchelt, H., 1987. Isotope geochemistry of Pacific mid-ocean ridge basalt. J. Geophys. Res., 92: 4881–4893.

Woodruff, L.G. and Shanks, W.C., III, 1988. Sulfur isotope study of chimney minerals and vent fluids from 21°N, East Pacific Rise: hydrothermal sulfur sources and disequilibrium sulfate reduction. J. Geophys. Res., 93: 4562–4572.

Yeh, H. and Savin, S.M., 1977. Mechanisms of burial metamorphism of argillaceous sediments, 3. O-isotope evidence. Geol. Soc. Am. Bull., 99: 1321–1330.

Zierenberg, R.A. and Schiffman, P., 1990. Microbial control of silver mineralization at a sea-floor hydrothermal site on the northern Gorda Ridge. Nature, 348: 155–157.

Zierenberg, R.A., Shanks, W.C., III and Bischoff, J.L., 1984. Massive sulfide deposits at 21°N, East Pacific Rise: chemical composition, stable isotopes, and phase equilibria. Geol. Soc. Am. Bull., 95: 922–929.

Zierenberg, R.A., Shanks, W.C., III, Seyfried, W.E., Jr., Koski, R.A. and Strickler, M.D., 1988. Mineralization, alteration and subseafloor metamorphism of the ophiolite-hosted Turner-Albright sulfide deposit, southwestern Oregon. J. Geophys. Res., 93: 4657–4674.

Zierenberg, R.A., Schiffman, P., McClain, J., Jonasson, I.R., Tosdal, R. and Pickthorn, W., 1992. Magnesium metasomatism and silicification of basalt hyaloclastite at an active sea floor hydrothermal site on the Gorda Ridge, 42°45′N lat., Northeast Pacific Ocean. Conf. Int. Geol. Corr. Proj. 294: Very Low Grade Metamorphism, U.C. Davis, Abstr. Progr., 47.

Zierenberg, R.A., Koski, R.A., Morton, J.L., Bouse, R.M. and Shanks, W.C., III, 1993. Genesis of massive sulfide deposits on a sediment-covered spreading center, Escanaba Trough, 41°N, Gorda Ridge. Econ. Geol., 88: 2133–2162.